Sphingosine-1-phosphate activates mouse vagal airway afferent C-fibres via S1PR3 receptors

Mayur J. Patil[1], Sonya Meeker[1], Diana Bautista[3], Xinzhong Dong[2] and Bradley J. Undem[1]

[1]*Department of Medicine, Johns Hopkins University School of Medicine, Baltimore, MD, USA*
[2]*Department of Neuroscience, Johns Hopkins University School of Medicine, Baltimore, MD, USA*
[3]*Department of Molecular and Cell Biology, University of California, Berkeley, CA, USA*

Edited by: Ian Forsythe & David Grundy

Key points

- Sphingosine-1-phosphate (S1P) strongly activates mouse vagal C-fibres in the airways.
- Airway-specific nodose and jugular C-fibre neurons express mRNA coding for the S1P receptor S1PR3.
- S1P activation of nodose C-fibres is inhibited by a S1PR3 antagonist.
- S1P activation of nodose C-fibres does not occur in S1PR3 knockout mice.

Abstract   We evaluated the effect of sphingosine-1-phosphate (S1P), a lipid that is elevated during airway inflammatory conditions like asthma, for its ability to stimulate vagal afferent C-fibres in mouse lungs. Single cell RT-PCR on lung-specific vagal afferent neurons revealed that both TRPV1-expressing and TRPV1-non-expressing nodose neurons express mRNA coding for the S1P receptor S1PR3. TRPV1-expressing airway-specific jugular ganglion neurons also express S1PR3 mRNA. S1PR1 and S1PR2 mRNAs were also found to be expressed but only in a limited subset (32% and 22%, respectively) of airway-specific vagal sensory neurons; whereas S1PR4 and S1PR5 were rarely expressed. We used large scale two-photon imaging of the nodose ganglia from our *ex vivo* preparation isolated from *Pirt-Cre;R26-GCaMP6s* transgenic mice, which allows for simultaneous monitoring of calcium transients in ∼1000 neuronal cell bodies in the ganglia during tracheal perfusion with S1P (10 μM). We found that S1P in the lungs strongly activated 81.5% of nodose fibres, 70% of which were also activated by capsaicin. Single fibre electrophysiological recordings confirmed that S1P evoked action potential (AP) generation in a concentration-dependent manner (0.1–10 μM). Action potential generation by S1P in nodose C-fibres was effectively inhibited by the S1PR3 antagonist TY 52156 (10 μM). Finally, in S1PR3 knockout mice, S1P was not able to activate any of the airway nodose C-fibres analysed. These results support the hypothesis that S1P may play a role in evoking

C-fibre-mediated airway sensations and reflexes that are associated with airway inflammatory diseases.

Corresponding author Bradley Undem: Johns Hopkins University School of Medicine, 5501 Hopkins Bayview Circle, Room 3A44, Baltimore 21224, MD, USA.   Email: bundem@jhmi.edu

Introduction

The majority of vagal nociceptors in the airways are slow-conducting capsaicin-sensitive C-fibres. Activation of vagal C-fibres leads to reflex bronchoconstriction, mucus secretion and sensations of dyspnoea and urge-to-cough (Mazzone & Undem, 2016). It is well accepted that visceral and somatosensory C-fibres are activated by endogenous chemical mediators at sites of inflammation. In laboratory animals, activation of the vagal C-fibres during airway allergic inflammation by inflammatory mediators leads to the phenomenon of airway hyperreactivity (Trankner *et al.* 2014; McAlexander *et al.* 2015).

There is relatively little known about the nature of inflammatory molecules that lead to vagal C-fibre activation in the airways, or the mechanisms by which such activation occurs. There is a plethora of inflammatory mediators that arise at sites of airway inflammation, including cytokines, chemokines, amines, proteases, TLR agonists and lipid mediators. In order to prioritize those mediators most likely to directly interact with vagal C-fibres we recently carried out an RNAseq analysis specifically on capsaicin-sensitive C-fibre neurons isolated from the vagal jugular and nodose ganglia. In our analysis we noted that receptors for the vast majority of inflammatory mediators are not expressed by C-fibre neurons. Nevertheless, both nodose and jugular C-fibre neurons expressed receptors for a distinct profile of a limited number of inflammatory mediators that included sphingolipid receptors (Wang *et al.* 2017).

Sphingosine-1-phosphate (S1P) is a bioactive metabolite of sphingolipid, the ubiquitous building blocks of all mammalian cell membranes (Maceyka *et al.* 2012). S1P can act as an intracellular signalling molecule, but it can also be released to act as an autacoid. Extracellular S1P mediates its actions via five cognate G protein-coupled receptors S1PR1–S1PR5 (Hla, 2003). In the past two decades the role of S1P in regulating chronic inflammatory conditions like asthma, multiple sclerosis, rheumatoid arthritis and inflammatory bowel disease has received much attention (Maceyka & Spiegel, 2014). The importance of S1P specifically in airway inflammatory diseases can be underscored by elevated levels of S1P found in bronchoalveolar lavage (BAL) fluid of idiopathic pulmonary fibrosis and asthmatic patients (Ammit *et al.* 2001; Jolly *et al.* 2002; Ryan & Spiegel, 2008; Milara *et al.* 2012). In this study we use a single cell RT-PCR analysis

to show that virtually all of airway-specific vagal C-fibre neurons express S1P receptors, most notably, S1PR3. We combine this with two-photon GCaMP6 imaging and electrophysiological studies to show that S1P strongly activates action potential discharge from vagal C-fibre terminating in mouse lungs and that this activation requires S1PR3 receptor stimulation.

Methods

Ethical approval of animal experiments

All animal experiments were approved by the Johns Hopkins School of Medicine Animal Care and Use Committee. We as investigators understand the ethical principles under which the journal operates, and their work complies with the animal ethics checklist as described by Grundy (2015). Male mice (C57BL/6J) were purchased from Jackson Labs. The $S1Pr3^{-/-}$ mice were originally obtained from Jackson Labs (see Hill *et al.* 2018). The Pirt-Cre mice were generated in X. Dong's laboratory. The ROSA26-lsl-GCaMP6 line was originally provided by D. Bergles at The Johns Hopkins University. The animals were housed in an approved animal facility under a 12:12 h light/dark cycle with controlled temperature and humidity, in groups in cages providing unrestricted access to food and water and an appropriate environmental enrichment. The mice were I.P. injected with anti-coagulant heparin (2000 IU kg^{-1}; diluted in saline 1000 IU ml^{-1}). The injection of heparin is given to prevent blood clot formation and improves blood removal from the pulmonary circulation. After 15–20 min, the mice were killed by exposure to CO_2 in a rising concentration and exsanguination. The CO_2 was sourced from a compressed CO_2 gas cylinder and administered at a flow rate measured by a flow meter displacing 20–30% of the chamber volume per minute, conforming to requirements given in Grundy, (2015). The isolated preparations were studied at 37°C in Krebs bicarbonate solution (KBS); composed of (mM): 118 NaCl, 5.4 KCl, 1.0 NaH$_2$PO$_4$, 1.2 MgSO$_4$, 1.9 CaCl$_2$, 25.0 NaHCO$_3$ and 11.1 dextrose, gassed with air mix (95% O$_2$–5% CO$_2$, pH 7.4).

Retrograde labelling and cell dissociation

To collect lung-specific bronchopulmonary afferent neurons from jugular/nodose ganglia, the airways of

C57/BL6 mice (male, 8 weeks) were retrogradely labelled using DiI (Invitrogen, Thermo Fisher Scientific, Waltham, MA, USA) (1% DMSO diluted 1:10 in PBS). Under anaesthesia (2 mg ketamine and 0.2 mg xylazine I.P. per mouse), mice were orotracheally intubated, and 10–12 μl of DiI was instilled into the tracheal lumen 4–5 days before an experiment. The animals were killed by CO_2 asphyxiation, and the jugular/nodose ganglia were dissected and cleared of adhering connective tissue. Isolated ganglia were incubated in an enzyme buffer (2 mg ml^{-1} collagenase type 1A and 2 mg ml^{-1} dispase II in Ca^{2+}- and Mg^{2+}-free Hanks' balanced salt solution) for 30–60 min at 37 °C. Neurons were dissociated by trituration with three glass Pasteur pipettes of decreasing tip pore size, then washed by centrifugation (three times at 1000 g for 2 min) and suspended in L-15 medium containing 10% fetal bovine serum (FBS). The cell suspension was transferred onto poly-D-lysine/laminin-coated coverslips. After the suspended neurons had adhered to the coverslips for 2 h, the neuron-attached coverslips were flooded with the L-15 medium (10% FBS) and used within 8 h for cell picking.

Cell picking

Coverslips of retrogradely labelled, dissociated neurons were constantly perfused by Locke's solution and the labelled cells identified by using fluorescence microscopy. Single cells were sucked into a glass-pipette (tip diameter 50–150 μm) that was pulled with a micropipette puller (Model P-87, Sutter Instruments Co., Novato, CA, USA) by applying negative pressure. The pipette tip was then broken in a PCR tube containing 1 μl RNAse Inhibitor (RNAseOUT, 2 U μl^{-1}), immediately snap frozen and stored on dry ice. From one coverslip, one to four cells were collected. A sample of the bath solution from the vicinity of a labelled neuron was collected from each coverslip for no-template experiments (bath control).

Single-cell RT-PCR

The tubes with airway/lung-labelled jugular/nodose single cells suspended in RNAse OUT were used to synthesize first strand cDNA by using the SuperScript III First-Strand Synthesis System for RT-PCR (Cat. No. 18080044, Invitrogen, Carlsbad, CA, USA) according to the manufacturer's recommendations. In short, cell samples were defrosted and then oligo(dT) and random hexamer primers (Roche Applied Bioscience) were added and tubes incubated for 10 min at 75°C. A 22 μl aliquot of the volume was reverse transcribed by adding SuperscriptIII RT for cDNA synthesis, whereas water was added to the remaining sample, which was used as –RT control. PCR was performed as follows. A 1 μl aliquot (cDNA, RNA

Table 1. Single cell RT-PCR primer sequences

Gene	Primer	Sequence	Product length
β Actin	Forward (5′-3′)	CTG GTC GTC GAC AAC GGC TCC	302 bp
	Reverse (3′-5′)	GCC AGA TCT TCT CCA TG	
S1PR1	Forward (5′-3′)	TCT GCT CCT GCT TTC CAT CG	237 bp
	Reverse (3′-5′)	AGG ATG TCA CAG GTC TTC GC	
S1PR2	Forward (5′-3′)	CCT TCG TGG CCA ACA CCT TA	177 bp
	Reverse (3′-5′)	TGT CAC TGC CGT AGA GCT TG	
S1PR3	Forward (5′-3′)	ACC GCG TGT TCC TTC TGA TT	214 bp
	Reverse (3′-5′)	TTG ACC AGG CAG TAG ATG CG	
S1PR4	Forward (5′-3′)	GTG TAT GGC TGC ATC GGT CT	169 bp
	Reverse (3′-5′)	CCA CTA GGA TGA GGG CGA AG	
S1PR5	Forward (5′-3′)	TGT GTG TGC CTT CAT TGT GC	152 bp
	Reverse (3′-5′)	ACA GTA GGA TGT TGG TGG CG	
P2X2	Forward (5′-3′)	GGG GCA GTG TAG TCA GCA TC	241 bp
	Reverse (3′-5′)	TCA GAA GTC CCA TCC TCC A	
TRPV1	Forward (5′-3′)	TCA CCG TCA GCT CTG TTG TC	285 bp
	Reverse (3′-5′)	GGG TCT TGA ACT CGC TGT TC	

control or bath control) was used for PCR amplification of mouse β-actin, TRPV1, P2X2 and S1PR1-5 using the HotStar Taq Poymerase Kit (Qiagen) according to the manufacturer's recommendations in a final volume of 20 μl. After an initial activation step at 95°C for 15 min, cDNAs were amplified with custom-synthesized primers (Sigma-Aldrich) (Table 1) by 50 cycles of amplification. The PCR programme used was: denaturation at 94°C for 30 s, annealing at 60°C for 30 s and extension at 72°C for 1 min followed by a final extension at 72°C for 10 min. PCR products were then visualized in ethidium bromide-stained 1.5% agarose gels.

Two-photon imaging. The perfused vagal innervated tracheal-lung preparation was dissected from a mouse and set up as previously described (Kollarik et al. 2003). The trachea and lungs were isolated from *Pirt-Cre;R26-GCaMP6s* transgenic mice. The isolated

lungs were washed with KBS to wash the blood from the pulmonary circulation. A two-compartment chamber/tissue bath was used to mount the trachea and right lungs with intact right-side extrinsic vagal innervation including right jugular and nodose ganglia. The right nodose and jugular ganglia along with the vagus nerve were placed in one compartment, with the lung and trachea in the second compartment. The two compartments were separately superfused with KBS (4 ml min^{-1} at 37°C). There was no fluid exchange between the two compartments. The lung was pinned in one compartment (airway chamber) to receive chemical stimuli, while the trachea was cannulated with PE tubing, and both were continuously perfused with KBS (4 mL min^{-1}, respectively). The drugs were added to the receptive field in the lung via the trachea. The drugs applied in the lungs leave slowly in the perfusing buffer solution via small puncture ports made in the lungs and get immediately diluted into the superfusion buffer. The left or right vagal ganglia were pinned in a second compartment (VG chamber) for two-photon imaging. The chamber containing the tissue preparation was mounted on the microscope stage and fixed in place with two screws. The two chambers were then connected to buffer inlet lines perfusing warm buffer (37 °C), heated via Warner Instruments heating elements. The flow of KBS, gassed with air mix (95% O_2–5% CO_2, pH 7.4), was maintained at 4 ml min^{-1}. The 20× objective (Scientifica) was positioned directly above the nodose ganglia in the small chamber. Using Labview software, the ganglia coordinates for Z-stack, starting from top to bottom (100 μm), were adjusted. The piezo drive for the objective was engaged and the objective positioned at the top of the ganglia ready for image acquisition. We acquired live images of the nodose ganglia at 10 frames with 600 Hz frame scan mode per 6 s at a depth of ∼100 μm (10 planes of 10 μm thick slices). During the recordings we noticed that we could observe the activity of 1000 neurons in the ganglia. Our experiments revealed that ∼10% of the total neurons are lung-specific. In order to calibrate the two-photon system for our *ex vivo* preparation we carried out extensive electrical stimulation of the vagus nerve and analysed the Ca^{2+} transients to show that the intensity of the response is quasi-linear between 1 Hz and 10 Hz stimulation (when given in 5 s trains, data not shown). First, we recorded the baseline activity of the neurons without any stimulation and adjusted the laser power and emission gain (of the PMT) to record the lowest signal-to-noise ratio. The laser power and gain for our system were adjusted at 35% and 750 V, respectively. Next, we delivered 1 ml of buffer into the lungs and recorded the activity of neurons that were positive for distension. We marked these neurons during data analysis and did not include them in our drug response analysis. The two-photon set-up uses a laser excitation wavelength of 920 nm at which there is no

photobleaching of the GCaMP6 and hence no loss of signal over repetitive stimulation (Chen *et al.* 2013). The drugs were applied into the lungs via the tracheal cannula for 20 s. The drug response was recorded for a total of 3 min. The lungs were washed with 2 ml of KBS in between every drug application. The baseline for analysis was recorded 10 s before every drug application. The number of responding neurons were counted as those that have fluoresce intensity of > 1.5-fold over baseline. The software recorded images in tiff files that were analysed offline using ImageJ. Data are presented as $\Delta F/F_0$, the change in fluorescence intensity from baseline.

Two-photon imaging data analysis. The nodose ganglia were imaged up to a depth of 100 μm. The 100-μm depth was imaged in increments of 10 μm (1 plane). So altogether 10 planes were imaged in 6 s (per cycle). Typically, 1 cycle of images were collected as baseline (F_0) before any drug was applied. Images were collected for ∼2–5 min during drug application. All images were exported as tiff files to ImageJ for offline analysis. The first step in ImageJ was to open the Z-stacks of the various applications individually and observe the time lapse images using group Z-stack compression. This observation revealed if there was any X-, Y- or Z-axis movement of the ganglia during recording. Any movement of the ganglia during recording was corrected using an ImageJ plugin Stackreg. Next the Z-stacks for multiple drug analysis were concatenated (stitched) together in the sequence they were applied. The concatenated images were then divided or separated into substacks (each Z-stack was divided by 10 to create a substack) which were separated by 20 μm. The 20-μm separation was chosen as it gave enough separation between stacked neurons in the ganglia (mouse sensory neurons are approximately 20-μm in diameter). Thus 5 substacks out of the 10 were analysed, which ensured the same neurons were not counted twice. The substacked images were used to mark the ROIs (responsive neurons) and the intensity values collected and then analysed further in excel to calculate the $\Delta F/F_0$ value (change in fluorescent intensity from baseline).

Extracellular recording. The innervated isolated trachea-lung preparation was prepared as described above and previously (Kollarik *et al.* 2003). Action potentials were recorded at the level of the cell body strategically positioned in the vagal sensory ganglion using a sharp extracellular glass electrode filled with 3 M NaCl (impedance 2 MΩ). The recorded action potentials were amplified (Microelectrode AC amplifier 1800; A-M Systems, Everett, WA, USA), filtered (0.3 kHz of low cut-off and 1 kHz of high cut-off), and monitored on an oscilloscope (TDS340; Tektronix, Beaverton, OR, USA) and a chart recorder (TA240; Gould, Valley View,

OH, USA). The scaled output from the amplifier was captured and analysed by a Macintosh computer using NerveOfIt software (Phocis, Baltimore, MD, USA). For measuring conduction velocity, an electrical stimulation (S44; Grass Instruments, Quincy, MA, USA) was applied on the core of the receptive field. The conduction velocity was calculated by dividing the distance along the nerve pathway by the time delay between the shock artifact and the action potential evoked by electrical stimulation. If a C-fibre (<1 ms^{-1}) was found, the recording was started. C-fibres were stimulated by 1 ml of vehicle, α,β,mATP (10 μM), sphingosine-1-phosphate (S1P; 0.1, 1 and 10 μM), or capsaicin (CAP; 1 μM) injected into the lung through the trachea.

Drugs and solutions. All compounds and drugs used were freshly prepared, from 10 mM stock solutions stored at -20 °C, in Krebs solution to their final working concentration on the day of the experiment. The stock solutions of α,β,mATP, S1P, capsaicin and TY 52156 were prepared in distilled water, phosphate buffered saline with 4 mg ml^{-1} bovine serum, ethanol and DMSO, respectively.

Statistical analysis. The single fibre recording data are presented as a total number of APs evoked by indicated stimuli and expressed as means $\pm$ SEM. The two-photon data are presented as the mean intensity of activated neurons in presence of indicated stimuli and expressed as means $\pm$ SEM. The statistical tests used are indicated in the figure legends as appropriate.

Results

Airway-specific vagal sensory neurons express S1PR3

We previously employed an RNAseq analysis to show that S1PR3 is strongly expressed in mouse vagal sensory neurons (Wang *et al.* 2017). To determine if vagal capsaicin-sensitive C-fibre neurons specifically innervating the airways express S1P receptors we performed single cell RT-PCR on individual TRPV1-expressing (C-fibres) neurons labelled by the retrograde tracer DiI, previously instilled into mouse airways (schematic diagram in Fig. 1*A*). The nodose-jugular ganglion complex was collected from the mice 3 days after the tracer administration and RT-PCR performed from single labelled neurons collected from dissociated primary culture. The P2X2 gene was used as a marker of nodose neurons (*vs.* jugular neurons) (Nassenstein *et al.* 2010). A total of 31 single neurons (positive for β actin) were analysed for the presence of P2X2, TRPV1 and S1PRs 1–5. Out of the 31 neurons, 77% were nodose and 23% were jugular (based on presence or absence of P2X2). All of the nodose ganglia neurons analysed were S1PR3 positive

(Fig. 1*C*). Also, all of the TRPV1-positive jugular neurons (C-fibres) were positive for S1PR3 (Fig. 1*C*). Of the other S1P receptors, S1PR1 was in a total of 32% of neurons, S1PR2 was in 22% of neurons, whereas expression S1PR4 and S1PR5 was rare (Fig. 1*C* and *D*).

Sphingosine-1-phosphate activates airway nodose C-fibres

Previous studies of S1P in airway disease have dealt largely with its role in orchestrating the immune response (Jolly *et al.* 2002; Ryan & Spiegel, 2008; Maceyka & Spiegel, 2014). There is nothing known about the role of S1P in regulating airway afferent C-fibres. We adapted the *ex vivo* trachea-lung preparation that we have used for electrophysiological analysis of mouse vagal C-fibres (Kollarik *et al.* 2004) for two-photon imaging in *Pirt-Cre;R26-GCaMP6s* transgenic mice. In the *Pirt-Cre;R26-GCaMP6s* mice the pan-sensory neuronal *Pirt* promoter drives the expression of GCaMP6s in more than 95% of sensory neurons (Kim *et al.* 2014). This *Pirt-Cre;R26-GCaMP6s* transgenic mouse line offers the tool to record from the whole population of sensory neurons and has reproducible expression over generations (Anderson *et al.* 2018).

In order to calibrate the two-photon system for our *ex vivo* preparation we carried out extensive electrical stimulation studies of the vagus nerve and found that discharge of a single action potential leads to sufficient calcium entry to be detected by the microscope; the intensity of the response is essentially linear between 1 Hz and about 10 Hz stimulation, then saturates at higher frequencies (when given in 5 s trains, data not shown).

We performed all of our two-photon recordings by positioning the lens over the central aspect of the ganglion complex, a region that mostly consists of nodose ganglion neurons (Nassenstein *et al.* 2010). One of the major advantages of using two-photon microscopy on our *ex vivo* preparation is that we can track the responsiveness of each neuron to various different agonists during a single experiment, from application of buffer to α,β,mATP, S1P and then CAP. After application of a drug the lungs were washed out by perfusing with Krebs buffer. Before we started application of a drug, we recorded baseline fluorescence intensity (F_0), which we used to calculate the change in fluorescence intensity in the presence of the drug ($\Delta F/F_0$) (Supporting video S2). The baseline fluorescence in all our recordings of the nodose ganglia was very low. Application of 1 ml of S1P (10 μM) into the lungs for 2 min caused a robust action potential discharge, as depicted by the Ca^{2+} increases in nodose neurons (Fig. 2*D*, Supporting video S4). The mean intensity of the S1P response was similar in magnitude to the mean

intensity of the response to α,β,mATP and CAP, but the response was more persistent than the response to CAP (Fig. 3D). The neurons positive for α,β,mATP (agonist for P2X2,3 receptors) were considered as nodose in origin (Nassenstein *et al.* 2010). A total of 450 responsive neurons were recorded from 5 mice. The vast majority, 85%, of the responding nerve fibres were nodose in nature, most but not all of which were also sensitive to capsaicin, and the graph in Fig. 2F depicts only the percentages of nodose neurons. Neurons that are CAP positive and α,β,mATP negative are considered to be jugular C-fibres (Nassenstein *et al.* 2010). Around 56 neurons from our recordings can be considered as jugular C-fibres and 67% of these neurons were strongly S1P responsive.

To confirm that S1P effectively evokes action potentials from nodose C-fibres, and to obtain more detailed information on the frequency and pattern of action potential discharge we turned to a single fibre electrophysiological analysis using the same vagally innervated *ex vivo* trachea-lung preparation. We found that S1P evoked an action potential discharge in 28 of 30 nodose

C-fibres studied (CV averaged 0.63 ± 0.06 m s^{-1}) in a concentration-dependent manner (0.1–10 μM) (Fig. 3A and B). The response to 10 μM S1P was robust in that it evoked a greater number of total action potentials than CAP (1 μM; 377 ± 71 *vs* 192 ± 42; $P < 0.05$, $n = 13$ paired experiments). The peak frequency of discharge evoked by 10 μM S1P, however, was lower than that for capsaicin (6 ± 2 Hz *vs.* 22 ± 3 Hz, respectively; $P < 0.05$; Fig. 3D). The larger number of action potentials evoked by S1P was due to the response to S1P being more persistent (consistent with what we found with the GCaMP6s imaging study).

We evaluated the non-selective cation channel blocker Ruthenium Red at a concentration (30 μM for 15 min) known to block both TRPA1- and TRPV1-dependent responses in the mouse lungs. In two experiments S1P (10 μM) evoked 125 and 178 action potentials *vs.* 171 and 321 action potential before and after Ruthenium Red treatment. At the end of the experiment, in the presence of Ruthenium Red, capsaicin evoked only 46 and 69 action potentials in the two experiments.
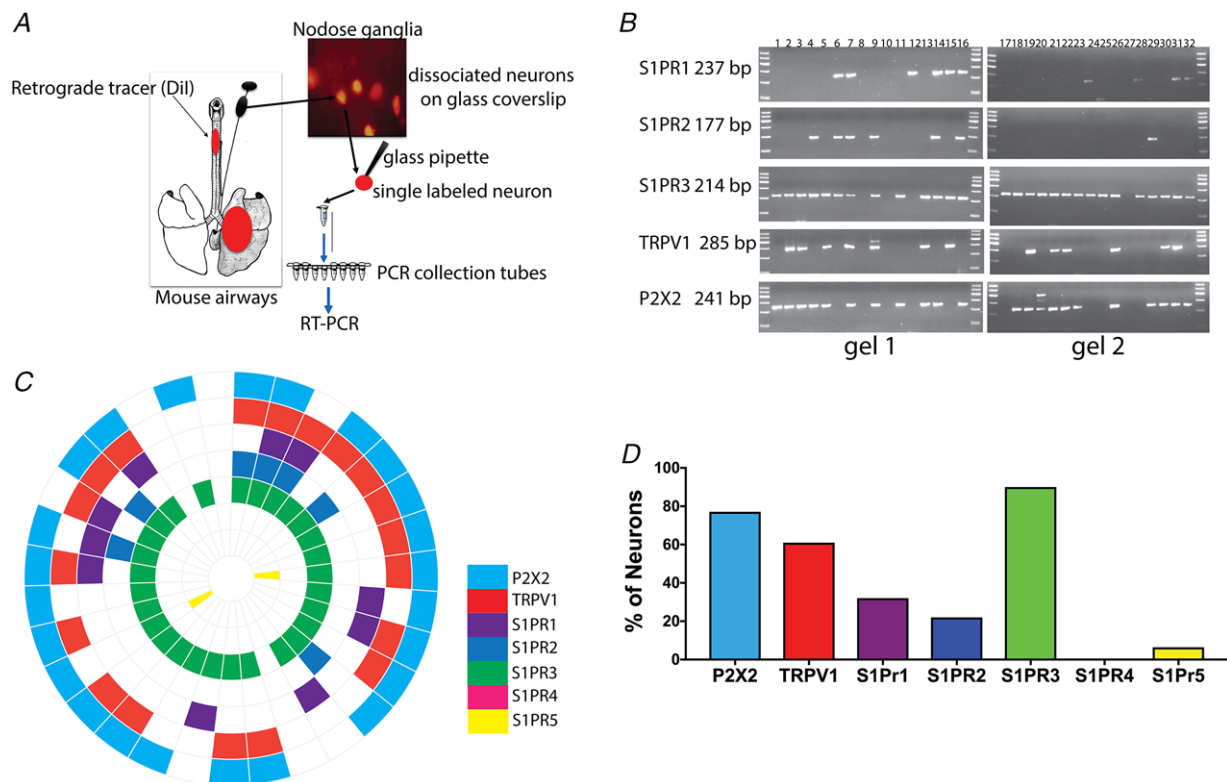
Figure 1. Airway-specific neurons express S1PR3
A, schematic diagram of labelling of the mouse airways with DiI tracer injected in the airways, DiI-labelled lung-specific neurons and picking of single labelled neurons to perform RT-PCR. *B*, agarose gels with PCR products of 31 (labelled 1–32, label 8 in all the gels is bath control) single labelled (lung-specific) neurons showing expression profile of S1PRs transcripts from mouse nodose and jugular ganglia. *C*, mRNA expression wheel summarizing expression profile of transcripts from 31 single neurons. Each section represents one neuron. *D*, bar graph showing percentage of neurons expressing P2X2 (77%), TRPV1 (61%), S1PRs 1 (32%), 2 (22%), 3 (90%), 4 (0%) and 5 (6.4%) mRNA ($n = 31$ single lung-specific neurons).
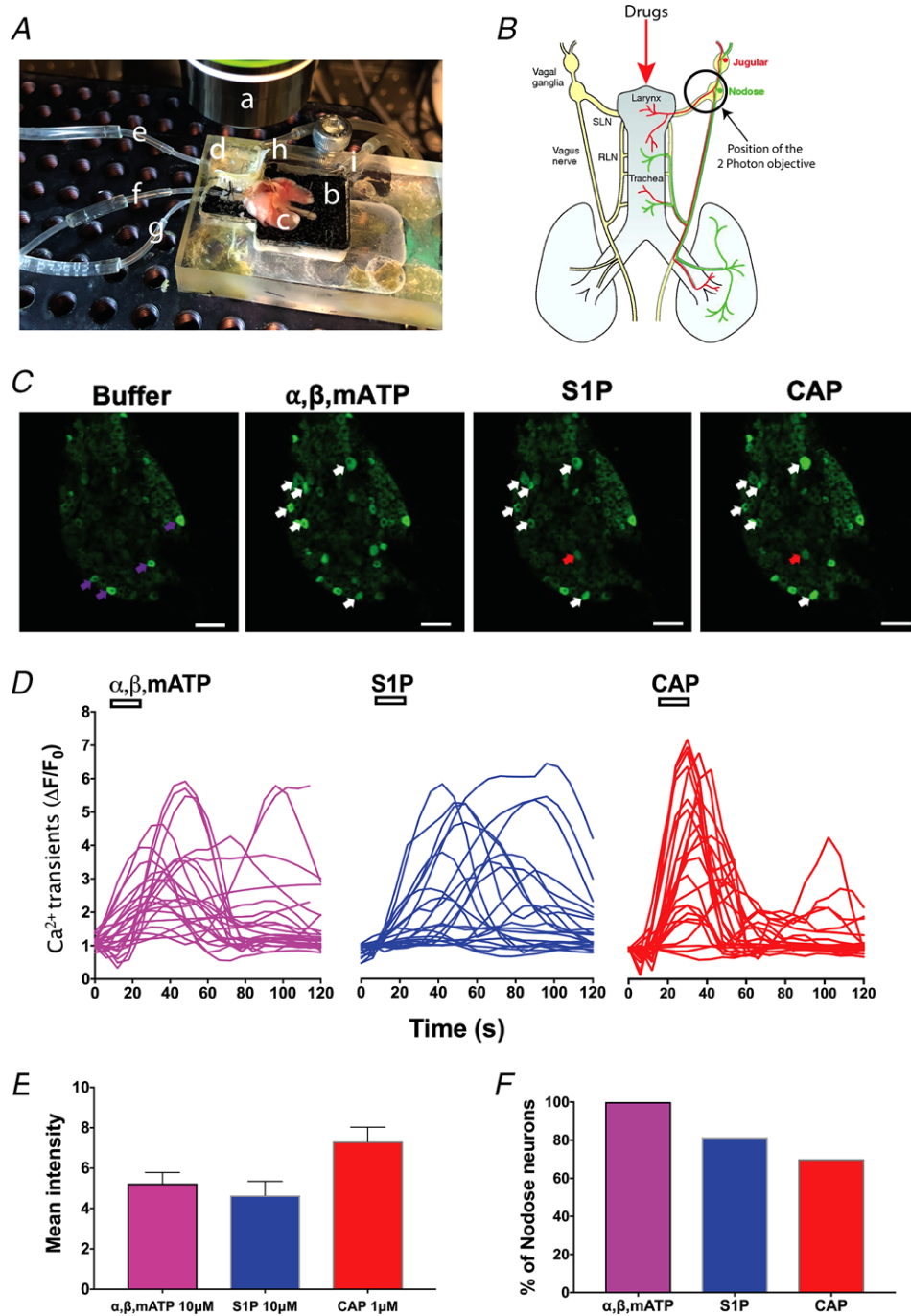
Figure 2. Activation of nodose ganglia neurons by sphingosine-1-phosphate visualized by two-photon microscopy

A, picture showing the imaging stage with the chamber containing a 20× water immersion objective (a), main chamber with warm Krebs solution (b), *ex vivo* lung with the trachea in the main chamber (c), small chamber with the vagal nerve and the vagal ganglia (d), ganglia chamber inflow line for warm Krebs solution (e), Krebs solution buffer and drug perfusion cannula attached to the trachea (f), main lung chamber inflow line for warm Krebs solution (g), outflow suction line for ganglia chamber (h), outflow suction line for main lung chamber (i). *B*, schematic diagram of the trachea, lung, vagus nerve and vagal ganglia, with a black circle showing the position of the two-photon objective on the nodose ganglia of the *Pirt-Cre;R26-GCaMP6* mice. *C*, images of one out of the 10 planes of the nodose ganglia from *Pirt-Cre;R26-GCaMP6* mice, recorded using two-photon microscope showing $[Ca^{2+}]_{in}$ increase (bright green) in nodose ganglia neurons, in the presence of buffer, α,β,mATP (10 μM), S1P (10 μM) and CAP (1 μM) (each application was for approximately 2 min) (Supporting videos S1, S2, S3 and

S4). Activated neurons are marked with an arrow, white arrows for neurons responding to α,β,mATP, S1P and CAP. Red arrows for S1P and CAP and purple arrows for mechanical distension sensitive neurons. All 4 images are of the same nodose ganglia and white bar represents 100 μm. *D*, representative traces of 20 neurons depicting time course of the calcium transients evoked by α,β,mATP (10 μM), S1P (10 μM) and CAP (1 μM) (total 450 neurons were recorded from 5 mice). The data are expressed as ΔF (F/F_0), which is the change in whole-cell fluorescence intensity from baseline (normalized to baseline) as a function of time. *E*, bar graph showing mean intensity values for α,β,mATP, S1P and CAP presented as means + SEM. *F*, bar graph showing percentage of only nodose responsive neurons (α,β,mATP responsive), S1P and CAP ($n = 450$ neurons from 5 mice recorded on separate days).

S1PR3 mediates sphingosine-1-phosphates activation of airway nodose neurons

Our single cell RT-PCR results showed that the S1PR3 receptor is expressed in all of the nodose ganglia C-fibre neurons. To test the hypothesis that the action of S1P on activating nodose C-fibres is dependent on S1PR3, we evaluated the effect of an S1PR3 antagonist TY 52156 (Hoffmann *et al.* 2015). Pre-treatment (continuous perfusion) of the lungs with TY 52156 (10 μM) for 15 min significantly reduced (by ~70%) the S1P-mediated action potential generation in nodose C-fibres (Fig. 4*A*).

We next evaluated the nodose C-fibre response in S1PR3 knockout mice. We found that in the S1PR3 KO mice S1P (10 μM) had virtually no effect on nodose C-fibres. Action potential discharge in nodose C-fibres from wild-type and S1PR3 animals averaged 229.5 ± 48 ($n = 8$) *vs.* 4 ± 2.7 ($n = 6$), respectively (Fig. 4*C*). To confirm that the absence of S1PR3 in the nodose C-fibres did not otherwise change the phenotype of the neurons, we evaluated the number

of action potentials mediated by α,β,mATP (10 μM), and CAP (1 μM). We found no significant difference in the APs mediated by either α,β,mATP or CAP in S1PR3 KO C-fibres (Fig. 4*C*).

Discussion

The data support the following conclusions. With respect to S1P receptor expression, airway-specific vagal neurons rarely express S1P4 or S1P5 and only about 25% of the neurons express S1PR1 or S1PR2. In contrast, S1PR3 mRNA is expressed in every airway-specific nodose neuron, as well as in most TRPV1-expressing jugular neurons. Secondly, applying S1P to the lungs leads to action potential discharge in vagal nodose and jugular C-fibres. Thirdly, the activation of airway nodose C-fibres is entirely secondary to stimulation of S1PR3 receptors.

The occurrence of S1PR3 receptors in mouse and human dorsal root ganglia has been reported by
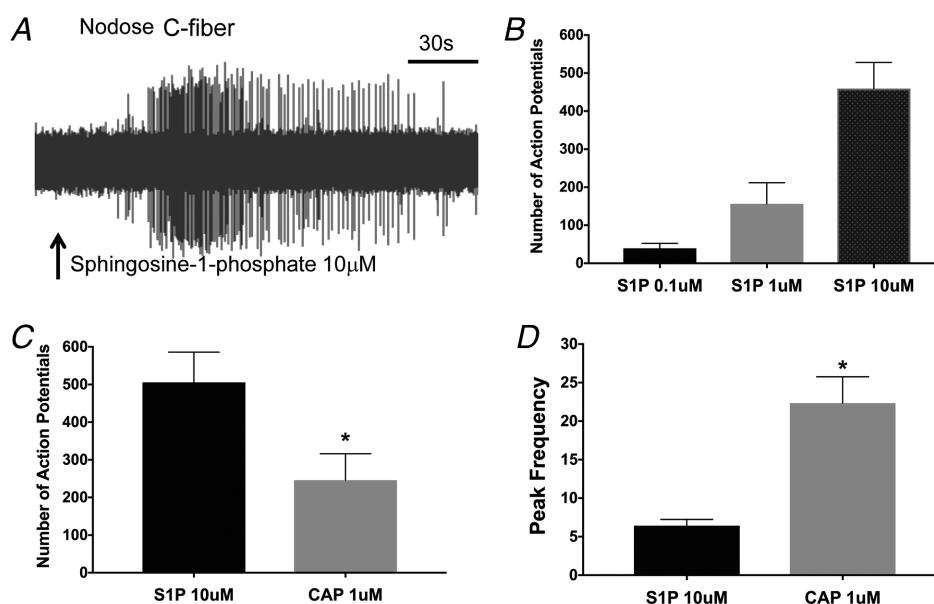
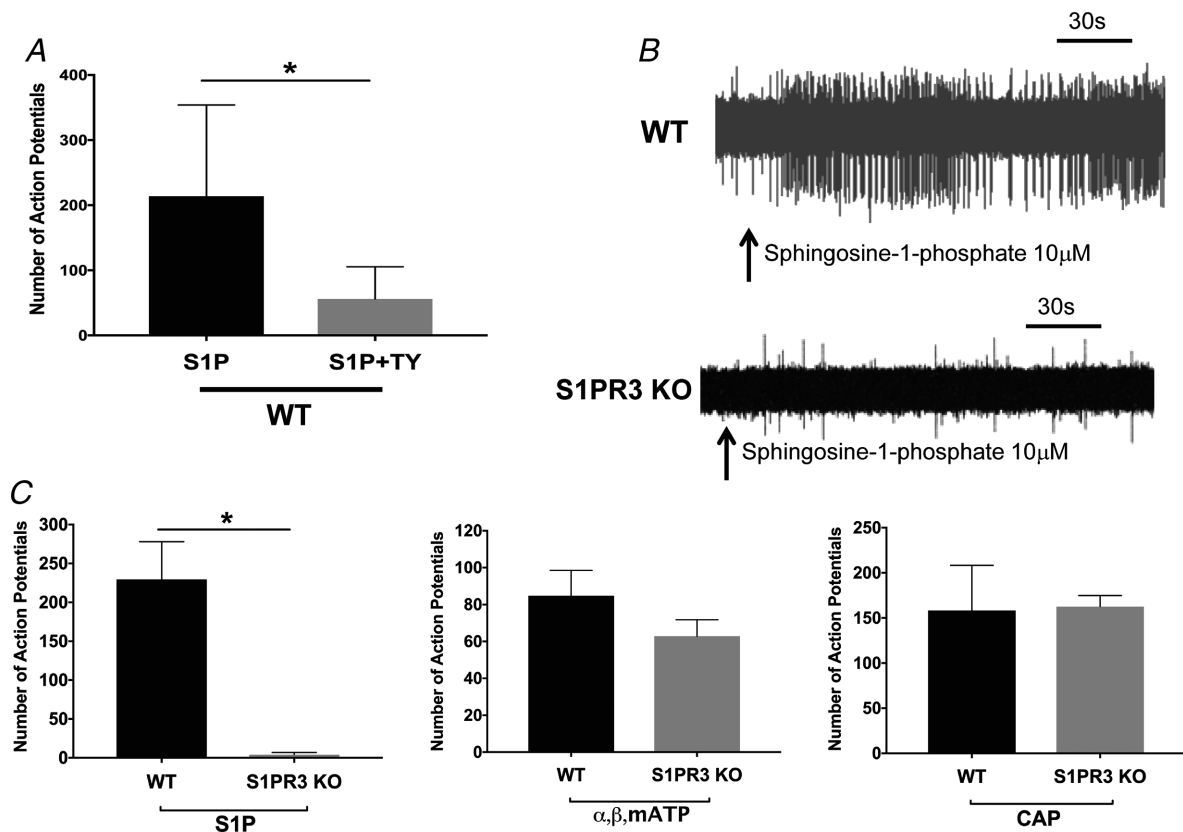**Figure 3. Sphingosine-1-phosphate activates airway nodose C-fibres**
A, representative tracing showing action potential discharge evoked by S1P (10 μM applied for approx. 2 min) in nodose C-fibre terminating in the mouse lung. *B*, graph showing total number of action potentials by nodose C-fibres in presence of 0.1, 1 and 10 μM concentrations of S1P ($n = 4$ for 0.1 μM, $n = 8$ for 1 μM and $n = 21$ for 10 μM). *C*, graph showing total number of action potentials by nodose C-fibres evoked by S1P (10 μM), and CAP (1 μM). *D*, the peak frequency of action potential discharge by S1P (10 μM), and CAP (1 μM) ($n = 10$). The data in bar graphs are presented as means + SEM.

various groups (Zhang *et al.* 2006; Mair *et al.* 2011; Camprubí-Robles *et al.* 2013; Hill *et al.* 2018). Trankner *et al.* (2014) were the first to note that S1PR3 was expressed in the mouse vagal sensory ganglion complex. S1P receptors have also been noted to be expressed in oesophageal-specific nodose and jugular vagal ganglion neurons in guinea-pigs (Yu *et al.* 2018). We previously noted in an RNAseq analysis specifically of capsaicin-sensitive vagal neurons isolated from the mouse nodose and jugular ganglia that among the five S1P receptor subtypes S1R3 was the most abundantly expressed, and that the expression was greater in nodose than jugular neurons (Wang *et al.* 2017). The results here with single cell RT-PCR analysis advance this knowledge further by showing that virtually all capsaicin-sensitive (TRPV1-expressing) neurons in the mouse nodose and jugular ganglion that specifically project to the respiratory tract express S1PR3 mRNA. In addition, TRPV1-non-expressing airway-specific nodose neurons, which are likely to comprise low mechanical threshold stretch receptors, i.e. slowly and rapidly adapting receptors, also expressed S1PR3 mRNA.

The development of GCaMP calcium indicator has provided a valuable tool for studying neuronal activity *in vivo* (Tian *et al.* 2009; Dana *et al.* 2014; Emery *et al.* 2016; Han *et al.* 2018). During our recordings of the nodose-jugular ganglia complex in our *ex vivo* trachea-lung preparation, we found that our two-photon imaging set-up confers the opportunity to successfully record from > 100 airway-specific neurons in each experiment out of the > 1000 neurons that are being imaged. The results with our high throughput GCaMP6s imaging indicates that S1PR mRNA expression confers function at the level of the nerve endings in the airways. The terminals of capsaicin-sensitive nodose and jugular fibres responded strongly with action potential discharge to S1P, as did a subset of capsaicin-insensitive nodose fibres. These results differ from those in the guinea-pig oesophagus where S1P activation was selective for jugular C-fibres (Yu *et al.* 2018).

Figure 4. S1PR3 mediates sphingosine-1-phosphates activation of airway nodose neurons
A, graph showing total number of action potentials evoked by S1P (10 μM) and S1P in the presence of S1PR3 antagonist TY 52156 ($n = 8$). Student's unpaired *t* test, *$P = 0.0159$ ($P < 0.05$). *B*, representative tracing showing action potential discharge evoked by S1P in nodose C-fibre from WT ($n = 8$) and S1PR3 KO ($n = 6$) mouse lung. *C*, graphs depicting total number of action potentials evoked by S1P (10 μM), $\alpha,\beta,$mATP (10 μM) and CAP (1 μM) in WT and S1PR3 knockout mice. Student's unpaired *t* test, **$P = 0.0018$ ($P < 0.05$). The data in bar graphs are presented as means + SEM.

The use of two-photon microscopy to evaluate the activity of sensory nerves can provide valuable information on thousands of neurons in a short period of time. The GCaMP6s indicator is well suited to detecting neuronal activation due to action potential discharge in that we noted it is sensitive enough to detect even a single action potential in a vagal afferent nerve, as has previously been noted in pyrimidal neurons (Chen *et al.* 2013). Nevertheless, this method does have a few limitations. The information on conduction velocities of individual fibres is lost. Although insights into relative intensity of action potential discharge can be obtained, information regarding the pattern of action potential discharge, action potential number and peak frequency cannot accurately be ascertained from two-photon GCaMP6s imaging. Also, when scanning the ganglion, the temporal resolution of the activation can be an issue wherein there is a possibility of missing out on some of the signal.

We used single fibre recording of afferent airway fibres to address the limitations in our imaging analysis. For these studies we focused on nodose C-fibres innervating the lungs. Our electrophysiological analysis satisfied the principle prediction from the imaging studies in that nodose C-fibres evoked action potential discharge in response to exposure to S1P. Capsaicin is one of the strongest activators of vagal C-fibres in the airways. With respect to intensity, as determined by peak frequency of discharge, the response to S1P was not as intense as capsaicin (6 Hz *vs.* 22 Hz, respectively) but a brief stimulation with S1P evoked a larger number of action potentials than capsaicin. This is explained by the observation, both in our imaging and single fibre recordings, that the response to S1P persisted for a longer period than the response to capsaicin.

We used our electrophysiological recordings to analyse the mechanism of S1P-induced activation of airway C-fibres. S1P can alter cellular function by acting either as an intracellular messenger (Ghosh *et al.* 1994), or by acting as an extracellular mediator via stimulation of S1P receptors (Hla, 2003). Since all nodose neurons expressed S1PR3 we hypothesized that the S1P-induced action potential discharge was secondary to stimulation of this GPCR. This hypothesis was supported both in a pharmacological analysis with an S1PR3 receptor antagonist, and also in a study evaluating S1P on nodose C-fibres in S1PR3 knockout mice. The S1PR3 antagonist TY 52156 strongly inhibited the response of nodose C-fibres to S1P. This antagonist has been identified and characterized fairly recently, and therefore its selectivity and specificity for S1PR3 has yet to be thoroughly scrutinized (Salomone & Waeber, 2011). In fact, at the concentration used, it can also inhibit S1PR4 receptors (Murakami *et al.* 2010). The results with S1PR3$^{-/-}$ supported the pharmacological analysis. Moreover, the results with S1PR$^{-/-}$ mice not only indicate that S1PR3

receptors are involved in the S1P response, but also that they are necessary for the response; i.e. in the absence of S1PR3 receptors, the S1P response was not just inhibited it was essentially abolished. That the responses of nodose C-fibres to capsaicin and $\alpha,\beta,$mATP were similar between S1PR3$^{-/-}$ and wild-type animals indicates the lack of response to S1P in the knockout animals was not due to a functional defect in the nerve fibres.

The ion channels subserving S1PR3 activation of airway C-fibre terminals are unknown. In the skin, S1PR3 activation leads to itch and pain responses that depend on TRPA1 and TRPV1 channels, respectively (Hill *et al.* 2018). Stimulation of bradykinin B2 receptors leads to action potential discharge in jugular C-fibres innervating the guinea-pig trachea, and this is partially inhibited by blocking TRPV1 receptors (Carr *et al.* 2003). Neither TRPV1 nor TRPA1 is necessary for S1P activation of nodose C-fibres in mouse lungs, as Ruthenium Red, at a concentration that strongly inhibited the response to TRPV1 stimulation with capsaicin (present study) and responses to TRPA1 stimulation with cinnamaldehyde (Nassenstein *et al.* 2008), did not inhibit the action potential discharge evoked by S1P.

S1P acting via S1PR3 (and also S1PR1) receptors have been previously shown to be important for nociceptor sensitization and inflammatory pain (Camprubí-Robles *et al.* 2013). The S1PR3 receptor has been implicated in S1P-induced nociceptor excitation and ongoing pain behaviour in mice and humans (Camprubí-Robles *et al.* 2013). Intracutaneous injection of S1P evokes itch (scratching) and pain in in mice. The itch is triggered by stimulating S1PR3 receptors in itch C-fibre neurons that in turn activate TRPA1 channels. Cutaneous pain is evoked by S1PR3 activation in a difference subset of neurons with the downstream activation of TRPV1 (Hill *et al.* 2018). There is little information on the role of S1P in evoking vagal afferent nerve-induced sensations or reflexes in the respiratory tract. The drug FTY720 (fingolimod) provides circumstantial evidence for a role of S1PR3 in human airway sensory nerve modulation. This drug is an agonist for S1PR1 and as such it is used mostly as an immunomodulator in the treatment of multiple sclerosis. FTY720 also activates S1PR3 (Brinkmann *et al.* 2002), and reported side-effects of its use include coughing and dyspnoea, sensations that can be evoked by activation of vagal afferent C-fibres in the airways; another side-effect potentially relevant to C-fibre activation is pain in the extremities (Kappos *et al.* 2006; Russo *et al.* 2015; Bianco *et al.* 2016; Rasenack *et al.* 2016).

S1P is elevated in the bronchoalveolar lavage in asthmatic subjects (Ammit *et al.* 2001). It is also well recognized to be released by the immunological activation of mast cells and can be a mediator in allergic diseases (Ammit *et al.* 2001; Roviezzo *et al.* 2004; Roviezzo *et al.* 2007; Chiba *et al.* 2010; Olivera & Rivera,

2011). This considered along with the information presented here, gives credence to the speculation that S1P via S1PR3 receptors may contribute to airway sensory neuro-modulation that is commonly associated with allergic inflammation (Taylor-Clark & Undem, 2006). In keeping with this, treating mice with S1P or FTY720 mimics respiratory allergen challenge, in that it leads to airways hyperreactivity (Roviezzo *et al.* 2004, 2010; Trifilieff & Fozard, 2012; Trankner *et al.* 2014). This is thought to depend on S1PR3 activation (Trifilieff & Fozard, 2012) and occurs in an animal model where the hyperreactivity is entirely dependent on the presence of vagal sensory C-fibre neurons (Trankner *et al.* 2014).

References

Ammit AJ, Hastie AT, Edsall LC, Hoffman RK, Amrani Y, Krymskaya VP, Kane SA, Peters SP, Penn RB & Spiegel S (2001). Sphingosine 1-phosphate modulates human airway smooth muscle cell functions that promote inflammation and airway remodeling in asthma. *FASEB J* **15**, 1212–1214.

Anderson M, Zheng Q & Dong X (2018). Investigation of pain mechanisms by calcium imaging approaches. *Neurosci Bull* **34**, 194–199.

Bianco A, Patanella AK, Nociti V, De Fino C, Lucchini M, Savio FL, Rossini PM & Mirabella M (2016). Severe dyspnoea with alteration of the diffusion capacity of the lung associated with fingolimod treatment. *Mult Scler Relat Disord* **9**, 11–13.

Brinkmann V, Davis MD, Heise CE, Albert R, Cottens S, Hof R, Bruns C, Prieschl E, Baumruker T, Hiestand P, Foster CA, Zollinger M & Lynch KR (2002). The immune modulator FTY720 targets sphingosine 1-phosphate receptors. *J Biol Chem* **277**, 21453–21457.

Camprubí-Robles M, Mair N, Andratsch M, Benetti C, Beroukas D, Rukwied R, Langeslag M, Proia RL, Schmelz M & Montiel AVF (2013). Sphingosine-1-phosphate-induced nociceptor excitation and ongoing pain behavior in mice and humans is largely mediated by S1P3 receptor. *J Neurosci* **33**, 2582–2592.

Carr MJ, Kollarik M, Meeker SN & Undem BJ (2003). A role for TRPV1 in bradykinin-induced excitation of vagal airway afferent nerve terminals. *J Pharmacol Exp Ther* **304**, 1275–1279.

Chen TW, Wardill TJ, Sun Y, Pulver SR, Renninger SL, Baohan A, Schreiter ER, Kerr RA, Orger MB, Jayaraman V, Looger LL, Svoboda K & Kim DS (2013). Ultrasensitive fluorescent proteins for imaging neuronal activity. *Nature* **499**, 295–300.

Chiba Y, Suzuki K, Kurihara E, Uechi M, Sakai H & Misawa M (2010). Sphingosine-1-phosphate aggravates antigen-induced airway inflammation in mice. *Open Respir Med J* **4**, 82–85.

Dana H, Chen TW, Hu A, Shields BC, Guo C, Looger LL, Kim DS & Svoboda K (2014). Thy1-GCaMP6 transgenic mice for neuronal population imaging in vivo. *PLoS One* **9**, e108697.

Emery EC, Luiz AP, Sikandar S, Magnusdottir R, Dong X & Wood JN (2016). In vivo characterization of distinct modality-specific subsets of somatosensory neurons using GCaMP. *Sci Adv* **2**, e1600990.

Ghosh TK, Bian J & Gill DL (1994). Sphingosine 1-phosphate generated in the endoplasmic reticulum membrane activates release of stored calcium. *J Biol Chem* **269**, 22628–22635.

Grundy D (2015). Principles and standards for reporting animal experiments in *The Journal of Physiology* and *Experimental Physiology*. *J Physiol* **593**, 2547–2549.

Han L, Limjunyawong N, Ru F, Li Z, Hall OJ, Steele H, Zhu Y, Wilson J, Mitzner W, Kollarik M, Undem BJ, Canning BJ & Dong X (2018). Mrgprs on vagal sensory neurons contribute to bronchoconstriction and airway hyper-responsiveness. *Nat Neurosci* **21**, 324–328.

Hill RZ, Hoffman BU, Morita T, Campos SM, Lumpkin EA, Brem RB & Bautista DM (2018). The signaling lipid sphingosine 1-phosphate regulates mechanical pain. *Elife* **7**, e33285.

Hla T (2003). Signaling and biological actions of sphingosine 1-phosphate. *Pharmacol Res* **47**, 401–407.

Hoffmann FS, Hofereiter J, Rubsamen H, Melms J, Schwarz S, Faber H, Weber P, Putz B, Loleit V, Weber F, Hohlfeld R, Meinl E & Krumbholz M (2015). Fingolimod induces neuroprotective factors in human astrocytes. *J Neuroinflammation* **12**, 184.

Jolly PS, Rosenfeldt HM, Milstien S & Spiegel S (2002). The roles of sphingosine-1-phosphate in asthma. *Mol Immunol* **38**, 1239–1245.

Kappos L, Antel J, Comi G, Montalban X, O'Connor P, Polman CH, Haas T, Korn AA, Karlsson G, Radue EW & Group FDS (2006). Oral fingolimod (FTY720) for relapsing multiple sclerosis. *N Engl J Med* **355**, 1124–1140.

Kim YS, Chu Y, Han L, Li M, Li Z, LaVinka PC, Sun S, Tang Z, Park K, Caterina MJ, Ren K, Dubner R, Wei F & Dong X (2014). Central terminal sensitization of TRPV1 by descending serotonergic facilitation modulates chronic pain. *Neuron* **81**, 873–887.

Kollarik M, Dinh QT, Fischer A & Undem BJ (2003). Capsaicin-sensitive and -insensitive vagal bronchopulmonary C-fibres in the mouse. *J Physiol* **551**, 869–879.

Kollarik M & Undem BJ (2004). Activation of bronchopulmonary vagal afferent nerves with bradykinin, acid and vanilloid receptor agonists in wild-type and TRPV1−/− mice. *J Physiol* **555**, 115–123.

McAlexander MA, Gavett SH, Kollarik M & Undem BJ (2015). Vagotomy reverses established allergen-induced airway hyperreactivity to methacholine in the mouse. *Respir Physiol Neurobiol* **212–214**, 20–24.

Maceyka M, Harikumar KB, Milstien S & Spiegel S (2012). Sphingosine-1-phosphate signaling and its role in disease. *Trends Cell Biol* **22**, 50–60.

Maceyka M & Spiegel S (2014). Sphingolipid metabolites in inflammatory disease. *Nature* **510**, 58.

Mair N, Benetti C, Andratsch M, Leitner MG, Constantin CE, Camprubí-Robles M, Quarta S, Biasio W, Kuner R & Gibbins IL (2011). Genetic evidence for involvement of neuronally expressed S1P1 receptor in nociceptor sensitization and inflammatory pain. *PLoS One* **6**, e17268.

Mazzone SB & Undem BJ (2016). Vagal Afferent innervation of the airways in health and disease. *Physiol Rev* **96**, 975–1024.

Milara J, Navarro R, Juan G, Peiro T, Serrano A, Ramon M, Morcillo E & Cortijo J (2012). Sphingosine-1-phosphate is increased in patients with idiopathic pulmonary fibrosis and mediates epithelial to mesenchymal transition. *Thorax* **67**, 147–156.

Murakami A, Takasugi H, Ohnuma S, Koide Y, Sakurai A, Takeda S, Hasegawa T, Sasamori J, Konno T, Hayashi K, Watanabe Y, Mori K, Sato Y, Takahashi A, Mochizuki N & Takakura N (2010). Sphingosine 1-phosphate (S1P) regulates vascular contraction via S1P3 receptor: investigation based on a new S1P3 receptor antagonist. *Mol Pharmacol* **77**, 704–713.

Nassenstein C, Kwong K, Taylor-Clark T, Kollarik M, Macglashan DM, Braun A & Undem BJ (2008). Expression and function of the ion channel TRPA1 in vagal afferent nerves innervating mouse lungs. *J Physiol* **586**, 1595–1604.

Nassenstein C, Taylor-Clark TE, Myers AC, Ru F, Nandigama R, Bettner W & Undem BJ (2010). Phenotypic distinctions between neural crest and placodal derived vagal C-fibers in mouse lungs. *J Physiol* **588**, 4769–4783.

Olivera A & Rivera J (2011). An emerging role for the lipid mediator sphingosine-1-phosphate in mast cell effector function and allergic disease. *Adv Exp Med Biol* **716**, 123–142.

Patel KN, Liu Q, Meeker S, Undem BJ & Dong X (2011). Pirt, a TRPV1 modulator, is required for histamin-dependent and -independent itch. *PLoS One* **6** e20559.

Rasenack M, Rychen J, Andelova M, Naegelin Y, Stippich C, Kappos L, Lindberg RL, Sprenger T & Derfuss T (2016). Efficacy and safety of fingolimod in an unselected patient population. *PLoS One* **11**, e0146190.

Roviezzo F, D'Agostino B, Brancaleone V, De Gruttola L, Bucci M, De Dominicis G, Orlotti D, D'Aiuto E, De Palma R, Rossi F, Sorrentino R & Cirino G (2010). Systemic administration of sphingosine-1-phosphate increases bronchial hyperresponsiveness in the mouse. *Am J Respir Cell Mol Biol* **42**, 572–577.

Roviezzo F, Del Galdo F, Abbate G, Bucci M, D'Agostino B, Antunes E, De Dominicis G, Parente L, Rossi F & Cirino G (2004). Human eosinophil chemotaxis and selective in vivo recruitment by sphingosine 1-phosphate. *Proc Natl Acad Sci U S A* **101**, 11170–11175.

Roviezzo F, Di Lorenzo A, Bucci M, Brancaleone V, Vellecco V, De Nardo M, Orlotti D, De Palma R, Rossi F, D'Agostino B & Cirino G (2007). Sphingosine-1-phosphate/sphingosine kinase pathway is involved in mouse airway hyperresponsiveness. *Am J Respir Cell Mol Biol* **36**, 757–762.

Russo M, Guarneri C, Mazzon E, Sessa E, Bramanti P & Calabro RS (2015). Fingolimod-associated peripheral vascular adverse effects. *Mayo Clin Proc* **90**, 1424–1427.

Ryan JJ & Spiegel S (2008). The role of sphingosine-1-phosphate and its receptors in asthma. *Drug News Perspect* **21**, 89–96.

Salomone S & Waeber C (2011). Selectivity and specificity of sphingosine-1-phosphate receptor ligands: caveats and critical thinking in characterizing receptor-mediated effects. *Front Pharmacol* **2**, 9.

Taylor-Clark T & Undem BJ (2006). Transduction mechanisms in airway sensory nerves. *J Appl Physiol* **101**, 950–959.

Tian L, Hires SA, Mao T, Huber D, Chiappe ME, Chalasani SH, Petreanu L, Akerboom J, McKinney SA, Schreiter ER, Bargmann CI, Jayaraman V, Svoboda K & Looger LL (2009). Imaging neural activity in worms, flies and mice with improved GCaMP calcium indicators. *Nat Methods* **6**, 875–881.

Trankner D, Hahne N, Sugino K, Hoon MA & Zuker C (2014). Population of sensory neurons essential for asthmatic hyperreactivity of inflamed airways. *Proc Natl Acad Sci U S A* **111**, 11515–11520.

Trifilieff A & Fozard JR (2012). Sphingosine-1-phosphate-induced airway hyper-reactivity in rodents is mediated by the sphingosine-1-phosphate type 3 receptor. *J Pharmacol Exp Ther* **342**, 399–406.

Wang J, Kollarik M, Ru F, Sun H, McNeil B, Dong X, Stephens G, Korolevich S, Brohawn P, Kolbeck R & Undem B (2017). Distinct and common expression of receptors for inflammatory mediators in vagal nodose versus jugular capsaicin-sensitive/TRPV1-positive neurons detected by low input RNA sequencing. *PLoS One* **12**, e0185985.

Yu X, Patil MJ, Yu M, Liu Y, Wang J, Undem BJ & Yu S (2018). Sphingosine-1-phosphate selectively activates vagal afferent C-fiber subtype in guinea pig esophagus. *Neurogastroenterol Motil* **30**, e13359.

Zhang YH, Fehrenbacher JC, Vasko MR & Nicol GD (2006). Sphingosine-1-phosphate via activation of a G-protein-coupled receptor(s) enhances the excitability of rat sensory neurons. *J Neurophysiol* **96**, 1042–1052.

Additional information

Competing interests

The authors declare that they have no competing interests.

Author contributions

M.J.P. and B.J.U. contributed to the conception or design of the study, acquisition, analysis or interpretation of data for the work, and drafting the manuscript or revising it critically for important intellectual content. D.B. provided S1PR3 KO mice. X.D. provided Pirt-cre/GCaMP6s mice and provided guidance with 2 photon microscope. M.J.P., S.M. and B.J.U. contributed to the acquisition, analysis or interpretation of data for the study, and drafting the manuscript or revising it critically for important intellectual content. All authors approved the final version of the manuscript, agree to be accountable for all aspects of the work in ensuring that questions related to the accuracy or integrity of any part of the work are appropriately investigated and resolved, all persons designated as authors qualify for authorship, and all those who qualify for authorship are listed.

Funding

Supporting information

Additional supporting information may be found online in the Supporting Information section at the end of the article.

Video S1. Nodose ganglia showing neurons getting activated (bright green) by α,β,mATP (10 μM) delivered in the lung compartment.

Video S2. Nodose ganglia showing neurons getting activated (bright green) due distention of the lung compartment by buffer (vehicle).

Video S3. Nodose ganglia showing neurons getting activated by (bright green) CAP (1 μM) delivered in the lung compartment.

Video S4. Nodose ganglia showing neurons getting activated (bright green) by S1P (10 μM) delivered in the lung compartment.

Figure S1. Agarose gel (2 tiers) showing PCR product of beta actin (302 bp). Each lane represents RT-PCR product from a single neuron. 100 bp ladder is loaded as a comparison on 2 ends of both tiers.

Figure S2. 2nd agarose gel showing PCR product of TRPV1 (285 bp). Each lane represents RT-PCR product from a single neuron. 100 bp ladder is loaded as a comparison on 2 ends of both tiers.

Figure S3. 1st agarose gel (2 tiers) showing PCR product of TRPV1 (285 bp). Each lane represents RT-PCR product from a single neuron. 100 bp ladder is loaded as a comparison on 2 ends of both tiers.

Figure S4. Agarose gel (2 tiers) showing PCR product of P2 × 2 (241 bp). Each lane represents RT-PCR product from a single neuron. 100 bp ladder is loaded as a comparison on 2 ends of both tiers.

Figure S5. Agarose gel (2 tiers) showing PCR product of S1PR1 (237 bp). Each lane represents RT-PCR product from a single neuron. 100 bp ladder is loaded as a comparison on 2 ends of both tiers.

Figure S6. Agarose gel (2 tiers) showing PCR product of S1PR2 (177 bp). Each lane represents RT-PCR product from a single neuron. 100 bp ladder is loaded as a comparison on 2 ends of both tiers.

Figure S7. Agarose gel (2 tiers) showing PCR product of S1PR3 (214 bp). Each lane represents RT-PCR product from a single neuron. 100 bp ladder is loaded as a comparison on 2 ends of both tiers.

Figure S8. Agarose gel (2 tiers) showing PCR product of S1PR4 (169 bp). Each lane represents RT-PCR product from a single neuron. 100 bp ladder is loaded as a comparison on 2 ends of both tiers.

Figure S9. Agarose gel (2 tiers) showing PCR product of S1PR5 (152 bp). Each lane represents RT-PCR product from a single neuron. 100 bp ladder is loaded as a comparison on 2 ends of both tiers.